Available online at www.sciencedirect.com

SciVerse ScienceDirect

Ceramics International 39 (2013) 3055–3064

CERAMICS INTERNATIONAL

www.elsevier.com/locate/ceramint

Effects of precursor, temperature, surface area and excitation wavelength on photoluminescence of ZnO/mesoporous silica nanocomposite

K. Sowri Babu*, A. Ramachandra Reddy, Ch. Sujatha, K. Venugopal Reddy

Department of Physics, National Institute of Technology Warangal, Warangal 506004, A.P., India

Received 9 August 2012; received in revised form 22 September 2012; accepted 25 September 2012
Available online 30 September 2012

Abstract

This paper reports on the effects of precursors, annealing temperature, surface area of host and excitation wavelength on photoluminescence (PL) of ZnO/mesoporous silica (MPS) nanocomposite. The samples were characterized with SAXRD, XRD, BET surface area and pore size analyzer, FE-SEM, HR-TEM, UV–vis absorption, FT-IR and PL spectrometers. The absorption band for ZnO nanoparticles embedded in MPS was detected at around 320 nm. A PL band positioned at around 393 nm has been observed in all the samples. Intensity of the PL band increased up to 550 °C and decreased when temperature reached to 700 °C. It is found that emission intensity enhanced along the rise in surface area of the host. This may be due to the enhancement in the density of Zn–O–Si bonds with increase in surface area. In addition, PL band is tuned from 393 nm to 504 nm by changing only the excitation wavelengths from 320 nm to 450 nm. The relationship between luminescence peak position and excitation wavelength is linear. This observation may be attributed to the size distribution of the particles and also a different distribution of different emissive sites on each passivated ZnO nanoparticle.

Keywords: ZnO nanoparticles; Photoluminescence; Red Edge Effect; Mesoporous silica

1. Introduction

The discovery of buckminsterfullerene brought great revolution in the field of nanoscience and technology [1]. These nanostructured materials has gained a lot of interest due to their potential applications in electronics, photonics, catalysis and sensing [2,3]. Among the various nanostructured materials available, ordered mesoporous silica materials attracted researchers due to their controllable pore size and shape. In the year 1992, first ordered mesoporous silica materials were invented by Mobil scientists [4]. Since then numerous studies have been reported concerning synthesis mechanisms, preparation conditions, characterization, and application of these materials as catalysts and catalyst supports in various reactions [5]. Besides this, these ordered mesoporous molecular sieves are also good candidates to host various semiconductor nanoparticles such as PbS, CdS, ZnS, TiO_2 and ZnO [6–11]. Recently much attention has also been paid to Eu^{3+} doped mesoporous silica and ferric oxide loaded mesoporous silica [12,13]. The pore size of these mesoporous silica materials can be tuned from 2 to 50 nm by using different templates. These materials are also available with different structures like hexagonal, cubic or lamellar phase [14]. The advantages of using these materials as hosts for semiconductor nanoparticles are, they efficiently prevent the agglomeration and also put the nanoparticles in sequential order [15]. ZnO semiconductor nanoparticles have gained much interest relative to other semiconductor nanoparticles due to variety of its applications in different fields.

The growing interest in ZnO is due to its applications as a gas sensor, transparent conductive films, surface acoustic waveguides, light-emitting diodes, field-emission, electronic/optical devices [16]. It has advantages over GaN because of

*Corresponding author. Tel.: +91 870 2462593, +91 9849171318; fax: +91 870 2430270.
E-mail address: sowribabuk@gmail.com (K. Sowri Babu).

0272-8842/$ - see front matter © 2012 Elsevier Ltd and Techna Group S.r.l. All rights reserved.
http://dx.doi.org/10.1016/j.ceramint.2012.09.085

its availability in bulk, single-crystal form and its larger exciton binding energy (~60 meV, cf. ~25 meV for GaN) [17]. ZnO is one of the semiconductors that show quantum confinement effect i.e. variation in band gap of semiconductor with particle size [8]. The first report on ZnO nanoparticles loaded in mesoporous silica MCM-41 was reported by Zhang et al. by functionalizing the surface of MCM-41 with ethylene diamine and later by Chen et al. [10,11]. Bao et al. proposed the formation of Zn–O–Si bonds in the ZnO/MPS nanocomposite prepared by impregnation method [18]. The existence Zn–O–Si bonds at the interface between ZnO and SiO_2 were proved by Fu et al. [19]. Later the long life time of photoluminescence of ZnO loaded inside MCM-41 was observed by Tang et al. [20]. The photoluminescence and photoelectric properties of ZnO/SiO_2 nanocomposite films prepared by electro deposition were studied by Gao et al. [21,22]. These ZnO/SiO_2 nanocomposite films exhibited significant blueshift which was ascribed to the quantum confinement effects of ZnO nanoparticles grown inside the mesochannels of SiO_2. It has also been observed that there is increased photoconductivity in ZnO/SiO_2 nanocomposite. Vaishnavi et al. have in situ prepared ZnO in the pores of mesoporous silica and detected two emission peaks at 355 nm and 405 nm [23]. A high ultraviolet emission was also observed by Burova et al. in ZnO/mesoporous silica nanocomposite compared to bulk ZnO [14]. Bouvy et al. investigated the structural and optical properties of ZnO and ZnS nanoparticles loaded in CMI-I nanocomposites by employing different synthesis methods [8,23–26]. The structural and optical properties of ZnO–SiO_2 nanocomposite films deposited by thermal evaporation and dip coating techniques were also studied [27,28]. Besides, doped ZnO and TiO_2 nanoparticles were also loaded in MCM-41 [29,30].

In this paper, the synthesis and detailed characterization of ZnO/MPS nanocomposite is reported. The effects of various parameters like precursor, temperature, surface area of host and excitation wavelength on PL of ZnO/MPS were studied. Interestingly, the PL spectrum is continuously shifted towards higher wavelength side with the increase of excitation wavelength.

2. Experimental procedure

Mesoporous silica (MPS) was prepared by the method reported by Grun et al. [31]. The preparation of ZnO/MPS nanocomposite was similar to the method described elsewhere [29]. To prepare ZnO/MPS nanocomposite, certain amount of zinc acetate/zinc nitrate was dissolved in 50 ml of ethanol and stirred at 80 °C for 2 h until it appeared clear and stable. To this solution, 4 ml of Triethanolamine (TEA) is added and stirred for 1 h and then 0.9 gm of MPS is added and stirred for another 0.5 h. To obtain the fine ZnO nanoparticles, Triethanolamine (TEA) has been used as catalyst and stabilizing agent. Finally, suitable quantity of water and ethanol mixture was added. The solution is stirred for 4 h and aged for 24 h. The resultant product was filtered, washed with ethanol several times. After this, sample was calcined in air at a rate of 2 °C/min and stayed at each temperature for 3 h to obtain ZnO/MPS nanocomposite. The above procedure was adopted in the synthesis of nanocomposites with amorphous nanosilica (ANS) and silica gel (SG). Commercially available silica gel (20–50 mesh) was used without further purification to make nanocomposite. The preparation of nanocrystalline silica is as follows: about 3.14 ml of aqueous ammonia (32 wt%) was added to a solution containing 74 ml of ethanol and 10 ml of deionized water. Eleven milliliters of TEOS was added to the above prepared mixture at 303 K with vigorous stirring and the reaction mixture was stirred continuously for 2 h to yield uniform silica spheres. The resultant product was retrieved by centrifugation and then calcined at 823 K for 6 h to produce ANS spheres.

3. Characterization

Small Angle X-ray powder diffraction (SAXRD) data were recorded on a Rigaku Ultima- IV diffractometer using Cu Kα (λ=1.5405 Å) radiation. To study the crystal structure of the MPS and ZnO/MPS materials, X-ray diffraction (XRD) experiments were carried out on Bruker D8 ADVANCE equipped with Cu K_α (λ=1.5405 Å) radiation with step size 0.049/sec. The surface areas of samples were measured by using Quntachrome NOVA 1200e BET (Braunner–Emmet–Teller) surface area and pore size analyzer at liquid nitrogen temperature (77 K). Morphology of the nanocomposite was studied by using a JEOL JSM 6390 Scanning Electron Microscope with high resolution of 3 nm and ZEISS FE-SEM having SEM Energy Dispersive Spectroscopy (EDS) attachment. To get the accurate particle size of ZnO nanoparticles embedded inside the pores of MPS, JEOL 3010 High Resolution Transmission Electron Microscope (HR-TEM) used. UV–vis absorption spectrometer was used to find absorption edge of ZnO nanoparticles incorporated in MPS. FT-IR spectra on KBr pellets were measured on a Bruker Optics FT-IR spectrometer Model: Tensor 27. The PL measurements were performed on Jobin Yuon spectrofluorometer, Model: FLUOROLOG-FL3-11 with wavelength resolution of 0.2 nm at room temperature. Xenon arc lamp of 450 W was used as the excitation light source to record excitation and emission spectra of samples. All PL spectra in this study were acquired by exciting the samples at an excitation wavelength of 320 nm.

4. Results and discussion

4.1. XRD and BET analysis

To confirm the mesoporous structure and effect of ZnO loading on it, SAXRD analysis was made on the samples. Fig. 1 depicts the SAXRD patterns of mesoporous silica and ZnO/MPS nanocomposite. The diffraction pattern of MPS exhibits a strong peak positioned at 2.33° and two

weak peaks located at 3.95° and 4.49°. These peaks are corresponding to the (100), (110) and (200) diffraction planes of hexagonal structure having long range order. The position of the (100) reflection is unaltered with the loading of ZnO in MPS matrix. It is confirmed that there is no change in pore size. The reduction in the main peak intensity of ZnO/MPS is due to the decrease of scattering contrast between pores content and silica walls [32]. The disappearance of the (110) and (200) reflections in the diffraction patterns of ZnO/MPS nanocomposite is due to decrease in the long range order of MPS. This could be assigned to the incorporation of ZnO nanoparticles in MPS matrix. Powder X-ray diffraction patterns of MPS and ZnO/MPS nanocomposite taken within the 2θ range of 10°–90° are shown in Fig. 2. These patterns show only diffuse peaks of non crystalline silica framework and no characteristic peaks of ZnO wurtzite structure have been observed. This shows that ZnO nanoclusters may be fully dispersed in MPS matrix. There is no information regarding the existence of ZnO nanoparticles and their size from XRD pattern of ZnO/MPS nanocomposite because the amorphous structure of MPS has totally quenched crystalline structure of ZnO. The structure of MPS has been confirmed from N_2-sorption isotherms measured from BET surface area and pore size analyzer and presented in Fig. 2. Type IV isotherm characteristic of mesoporous materials is obtained for both MPS and ZnO/MPS. With the incorporation of ZnO, the surface area of MPS drastically dropped from 952 m^2/g to 477 m^2/g and pore volume decreased from 0.63 to 0.29 cc/g. This suggests that ZnO is confined inside the pores of MPS.

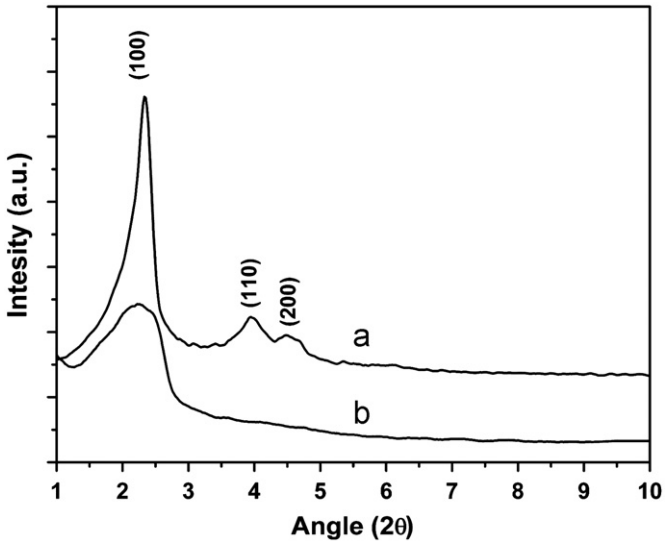

Fig. 1. Small angle X-ray diffraction (SAXRD) patterns of mesoporous silica (a) and ZnO/MPS nanocomposite (b).

4.2. Morphological analysis

Further, the morphology of ZnO/MPS was carefully investigated by FE-SEM. The FE-SEM picture and EDS measurements are shown in Fig. 3. These micrographs confirmed that the structure of MPS retained even after incorporation of ZnO. Ultimately, the presence of ZnO in the nanocomposite was revealed by SEM–EDS measurement which is shown in Fig. 3. The strong Zn signals were detected, confirming the presence of Zn element in the nanocomposite and Zn was present in all areas of MPS which was proved by HR-TEM analysis of the nanocomposite. Further, the existence of ZnO in the composite was also confirmed from PL spectrum. The HR-TEM images of MPS and ZnO/MPS nanocomposites are presented in Fig. 4(a) and (b). These pictures clearly demonstrate the encapsulation of ZnO nanoparticles in MPS matrix. ZnO nanocrystals homogeneously dispersed in the MPS matrix are clearly evidenced in Fig. 4(b). Most of the ZnO nanoparticles are very small in size and they are completely covered by the MPS network but some larger particles are visible as black dots in the image. The sizes of ZnO nanoparticles are ranging from 1.5 to 4 nm.

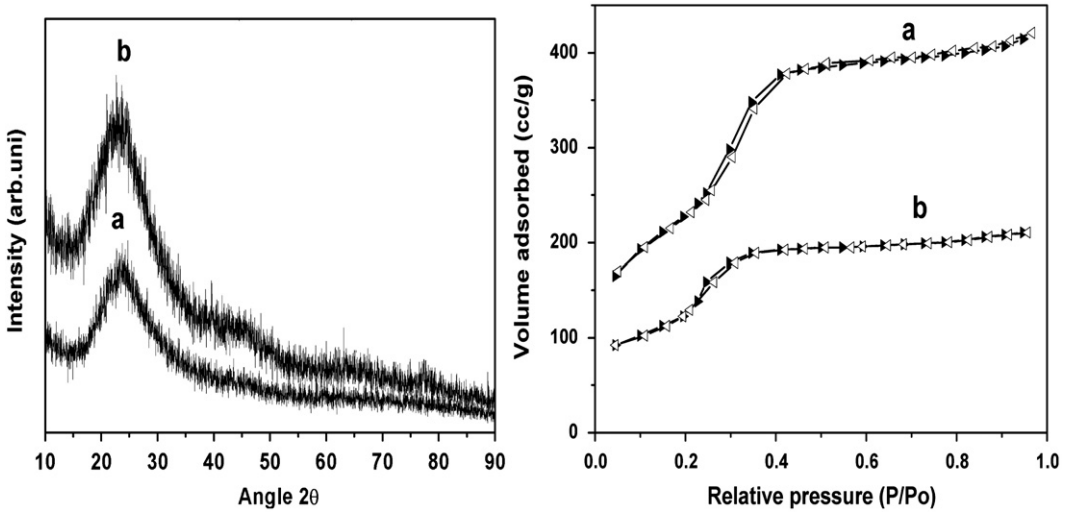

Fig. 2. X-ray diffraction patterns (left) and N_2-sorption isotherms (right) of MPS (a) and ZnO/MPS (b) nanocomposite.

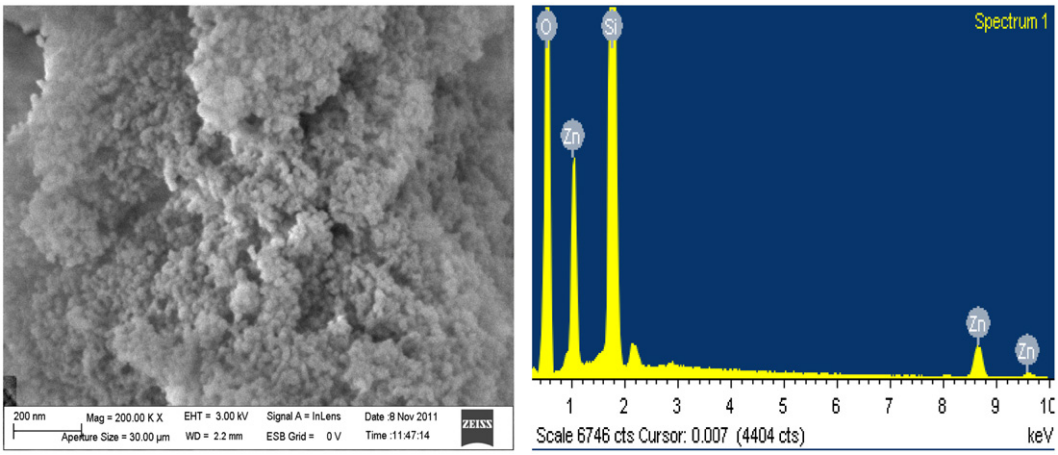

Fig. 3. FE-SEM image and EDS patterns of the ZnO/MPS nanocomposite recorded on FE-SEM.

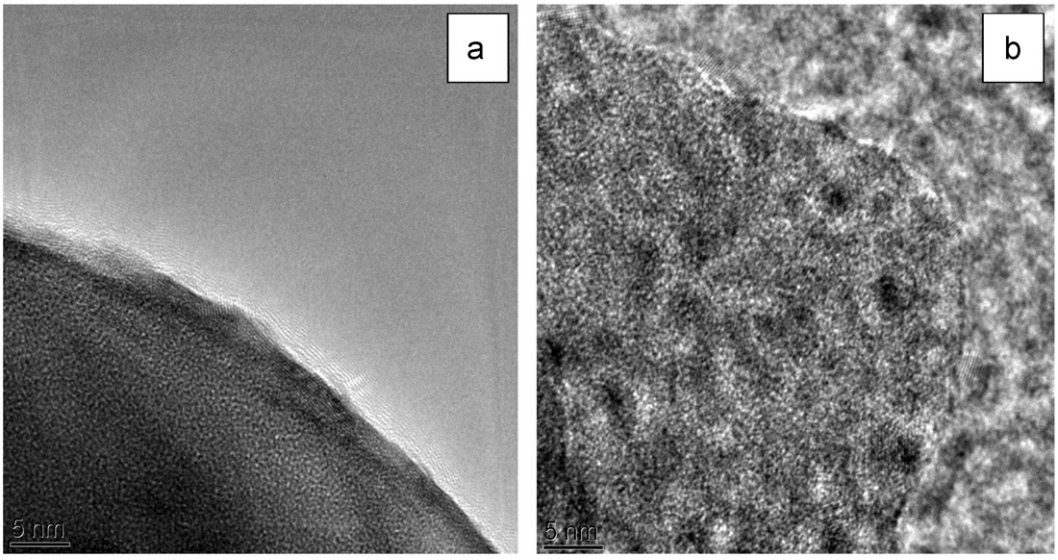

Fig. 4. HR-TEM images of the MPS and ZnO/MPS nanocomposite. Black regions in (b) are the ZnO nanoparticles embedded in MPS matrix.

4.3. UV–vis and FT-IR analysis

Fig. 4 shows the absorption spectra of ZnO/MPS nanocomposite. From Fig. 5(a), it can be seen that MPS shows absorption band at around 260 nm but when ZnO is loaded in MPS, the absorption spectrum represented two peaks one at 325 nm and the other one at 260 nm (Fig. 5(b)). The absorption band at 260 nm is attributed to the non-bridging oxygen hole centers [18]. Obviously, the absorption band at 325 nm is ascribed to the absorption of ZnO nanoparticles embedded in MPS matrix. It is strongly blueshifted to shorter wavelength side compared to the absorption of bulk ZnO whose absorption edge is located at 375 nm. This massive blueshift in the absorption spectrum shows the enhancement in the band gap due to quantum confinement effect of ZnO nanoparticles loaded in MPS. The infrared spectra of MPS and ZnO/MPS nanocomposite are presented in Fig. 6. The broad peak positioned at around 3450 cm^{-1} corresponds to stretching vibrations of –OH groups. Another distinct peak at around 1630 cm^{-1} observed is assigned to the bending modes of adsorbed water [33]. Two more bands at 1092 and 808 cm^{-1} are corresponding to asymmetric and symmetric modes stretching of Si–O–Si lattice vibrations [34]. The only difference between FT-IR spectra of MPS and ZnO/MPS nanocomposite is the disappearance of 962 cm^{-1} peak of MPS with ZnO loading [35]. These results are indicating that the loading of ZnO in MPS did not alter its structure.

4.4. Effect of precursor

PL spectra obtained from MPS and the samples prepared with zinc nitrate (S1) and zinc acetate (S2) precursors are shown in Fig. 7(a)–(c). The PL spectra of all samples were acquired at an excitation wavelength of 320 nm. MPS does

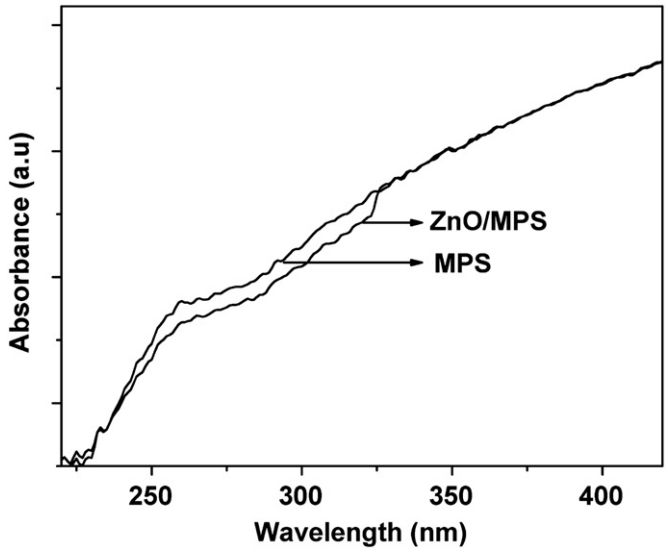

Fig. 5. UV–vis absorption spectrum of MPS and ZnO/MPS nanocomposite.

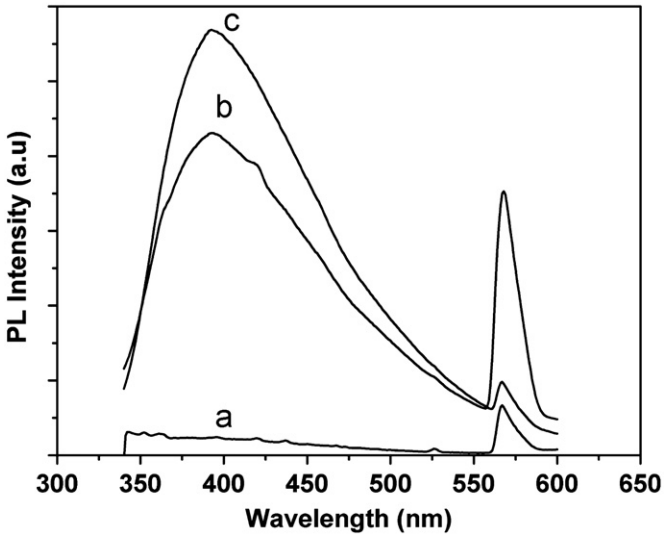

Fig. 7. PL spectra of MPS (a), ZnO/MPS nanocomposite prepared with zinc nitrate (b) and zinc acetate (c).

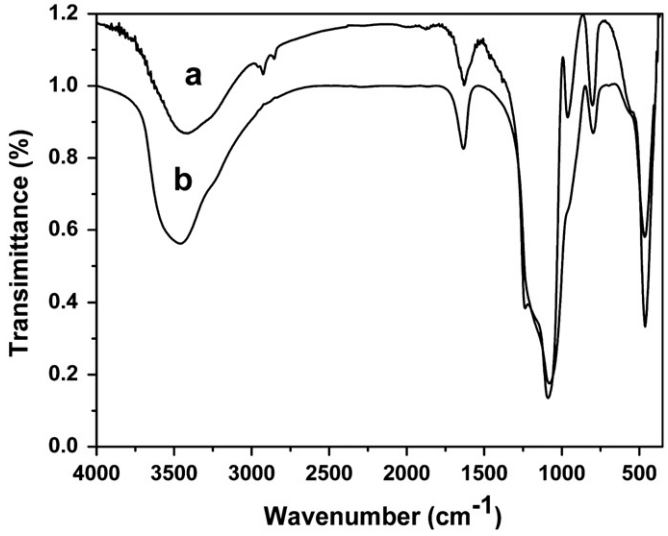

Fig. 6. FT-IR spectra of MPS (a) and ZnO/MPS nanocomposite taken on KBr pellets.

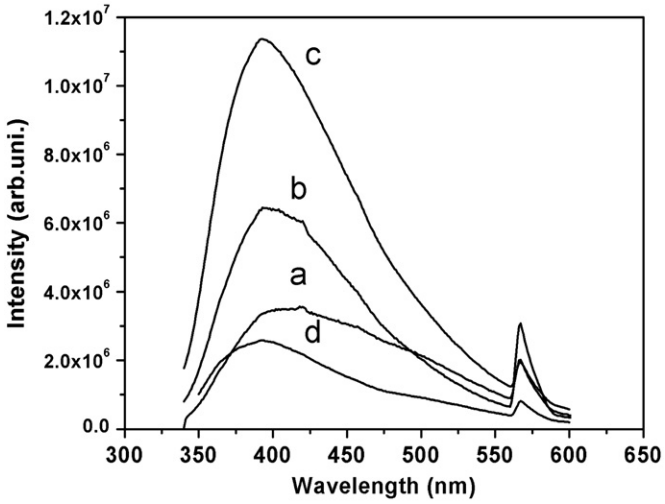

Fig. 8. PL spectra of ZnO/MPS nanocomposite (prepared with zinc acetate) calcined at 300 °C (a), 450 °C (b), 550 °C (c) and 700 °C (d).

not contributed to any luminescence in our study so the strong and broad emission peak positioned at 395 nm is due to emission from the ZnO nanoparticles. It can be seen from the figure that the intensity of nanocomposite prepared with zinc acetate is greater than nanocomposite made with zinc nitrate, the reason being, that NO_3 could provide more oxygen than CH_3CO_3 during the calcination process, consequently the defects associated with oxygen vacancies decreased [20]. A kink at 363 nm is visible in the UV region of PL spectrum of S1 which is attributed to the excitonic emission of ZnO nanoclusters loaded in MPS. It confirms the quantum confinement effect of ZnO nanoparticles encapsulated in MPS. The detailed analysis of the PL spectra was made in later sections.

4.5. Effect of temperature on PL

The PL spectra of samples calcined under different temperatures (350 °C, 450 °C, 550 °C and 700 °C) are shown in Fig. 8. With increase in temperature, the emission intensity of the PL band of nanocomposite increased monotonously until 550 °C and decreased beyond this temperature. Since the broad PL band is asymmetrical, it can be inferred that the PL band should have more than one origin. The Gaussian fitting was made carefully to find the various emission peaks contained in these broad PL spectra. Each spectra show four PL peaks among them three peaks are related to ZnO/MPS nanocomposite. A sharp peak at 568 nm was detected in all these samples.

Table 1
Gaussian fitting results of experimental PL spectra of the ZnO/MPS nanocomposite calcined at different temperatures.

Temperature (°C)	Peak 1 (nm)	Peak 2 (nm)	Peak 3 (nm)	R^2
300	385	420	478	0.99
450	380	415	465	0.99
550	377	412	462	0.99
700	382	422	487	0.99

R^2: Fitting regression coefficient.

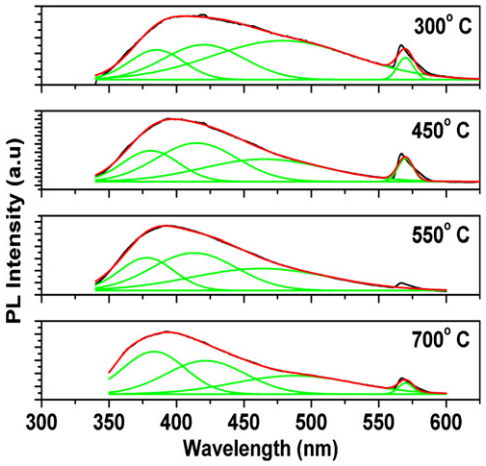

Fig. 9. Gaussian fitted PL spectra of samples calcined at different temperatures.

To know the origin of this peak, the PL spectra of MCM-41 and ZnO were also recorded. In both the samples, this peak was observed and no impurities were detected in the SEM–EDS measurement of samples. Finally, the PL of sample holder without sample was also recorded which shows three peaks positioned at 363 nm, 420 nm and 568 nm. Two peaks at 363 and 420 nm have not been appeared because of the high intensity of the samples. Table 1 summarizes the peak positions and their variation with increase in temperature. The continuous blueshift of all emission peaks with temperature indicates the reduction in particle size up to 550 °C. When annealing temperature was reached to 700 °C, there is an increase in the size of the ZnO nanoparticles; as a result, emission peaks were red-shifted. These results indicate the optimum annealing temperature 550 °C for ZnO/MPS nanocomposite. But larger ZnO nanocrystals with same surface passivation (calcined at 550 °C) were found to exhibit high PL intensity [29]. The reason for the decrease in intensity at 700° C is as follows. As the temperature was increased, the reduction atmosphere in pores became weak and more perfect ZnO crystallites were formed and hence there is decrease in PL intensity [11]. All the spectra contain three emission peaks. The emission peak at 377 nm is ascribed to the radiative transition in electron–hole recombination process [11] and other peaks at 412 nm and 462 nm are originated due to the oxygen vacancies at the interface between ZnO and SiO_2 and to the oxygen vacancies in the inner ZnO crystallites [11,27,29]. The decrease in PL intensity when sample was annealed at 700 °C represents the compensation of oxygen vacancies at the interface as well as in inner ZnO crystallites. It can also be seen in Fig. 9. that the relative intensity of the band edge emission is greater than the intensity of other emission peaks compared to the samples calcined at temperatures below 700 °C. This gives the evidence for the improved crystallanity of ZnO nanocrystals at higher temperatures.

4.6. Effect of surface area of Host

In this section, it is demonstrated the effect of surface area of host on PL of ZnO/MPS nanocomposite. For comparison, apart from the MPS which is having very high surface area (952 m^2/g), nanocrystalline silica and silica gel having surface areas of 150 m^2/g and 350 m^2/g were selected. The FE-SEM images of samples prepared with MPS, SG and ANS are shown in Fig. 10. All the three composites have shown spherical particles with different sizes. The PL spectra of ZnO/ANS, ZnO/SG and ZnO/MPS nanocomposites are shown in Fig. 11. It was found that intensity of PL spectra enhanced with increase in surface area. In ZnO/ANS the excitonic emission at 363 nm was observed. Obviously, the UV emission peak centered at 363 nm should be ascribed to the radiative transition in electron–hole recombination process [15]. Usually, ZnO exhibits the UV near band edge emission peak at around 380 nm along with the green emission located at around 530 nm. If the size of the ZnO nanoparticles decreased in the order of Bohr radius, nanoparticles exhibit quantum confinement effects i.e the band gap of quantum dot increase with a decrease in particle size. Consequently, the band edge emission in PL spectrum shows blueshift.

Z. Fu et al. suggested three phenomenon's responsible for enhancement in emission intensity in ZnO nanoparticles loaded in porous SiO_2 [19]. They are surface passivation of ZnO nanoparticles, formation of interface states between ZnO and SiO_2 and excitation process in the SiO_2. The absence of well known green emission band in all the three nanocomposites is an indication of the successful surface passivation of ZnO nanoparticles with all the three hosts ANS, SG and MPS used here. From the PL of ZnO/MPS, it can be concluded that the contribution of surface passivation of ZnO nanoparticles to PL enhancement is not significant in this case. To verify the contribution of

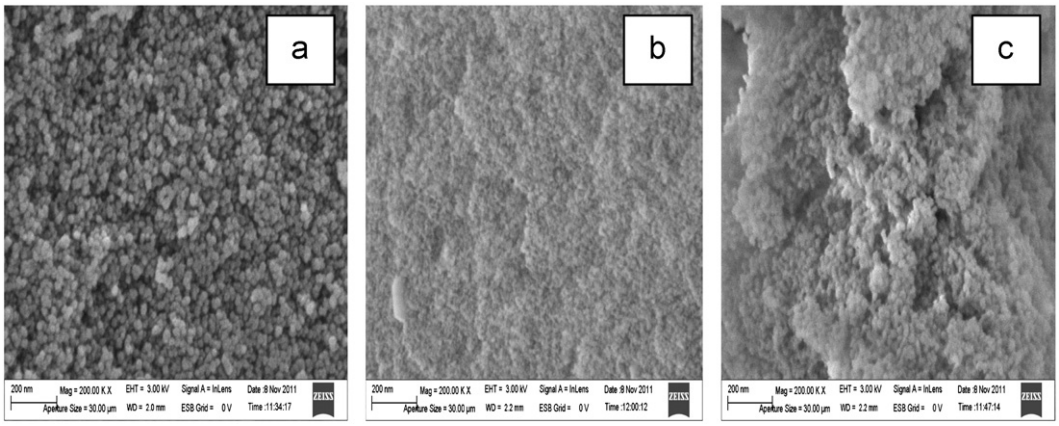

Fig. 10. FE-SEM images of ZnO/ANS (a), ZnO/SG (b) and ZnO/MPS (c) nanocomposites.

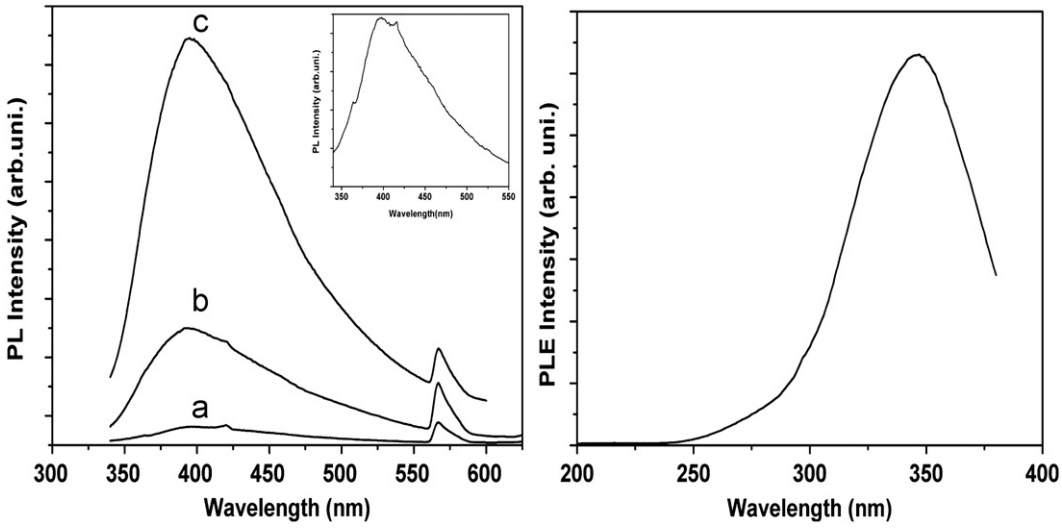

Fig. 11. PL spectra of nanocomposites ZnO/ANS (a), ZnO/SG (b), and ZnO/MPS (c). The graph on right side is the PL excitation spectrum of ZnO/MPS nanocomposite.

excitation processes in the SiO_2, the Photoluminescence Excitation (PLE) spectrum of the composite was recorded and is shown in Fig. 11. The PLE spectrum of ZnO/MPS nanocomposite depicts only a broad peak which is merely due to excitation processes in ZnO nanoparticles. So the role of excitation processes in MPS became negligible. The high PL intensity of the composite can be attributed to the formation of interface states where carriers can be trapped and recombine to emit. These interface states were increased with increase in surface area of the host matrix and hence there is a rise in PL intensity.

4.7. Effect of excitation wavelength

The PL spectra of ZnO/MPS nanocomposite that are taken at different excitation wavelengths can be seen in Fig. 12. With increase in excitation wavelength from 320 nm to 450 nm with an interval of 15 nm, PL spectrum of ZnO/MPS nanocomposite was continuously shifted from 393 nm to 504 nm. This type of unusual behavior is termed as red-edge effect (REE) as there is redshift in emission peak with respect to excitation wavelength [36]. To the best of our knowledge, it is the first report on excitation wavelength dependent phenomenon (EWDP) in ZnO/MPS nanocomposites. In general, the emission intensity decreases with increase in excitation wavelength. But in this case there is no significant decrease in emission intensity when the excitation wavelength was changed from 320 nm to 370 nm. The emission intensity reached its maximum value when the excitation wavelength is 355 nm. The reason being that, this wavelength is close to the excitation wavelength of the nanocomposite i.e. 347 nm which is shown in Fig. 11. But for excitation wavelengths above 370 nm, intensity decreased monotonously. But according to Kasha's rule, the same fluorescence emission spectrum is generally observed irrespective of the excitation wavelength [37]. This unusual EWDP has been extensively studied in the case of carbon

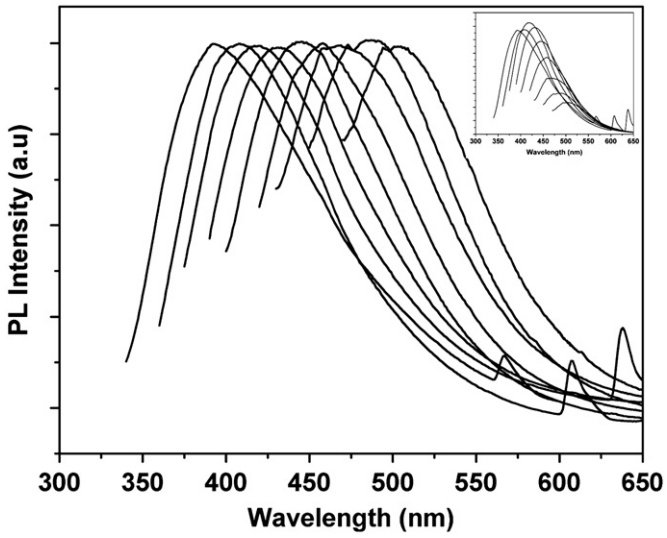

Fig. 12. PL spectra of the sample taken under different excitation wavelengths i.e. at 320, 340, 355, 370, 385, 400, 415, 430 and 450 nm. The inset graph shows the intensity variation of emission spectra with respect to change in excitation wavelength.

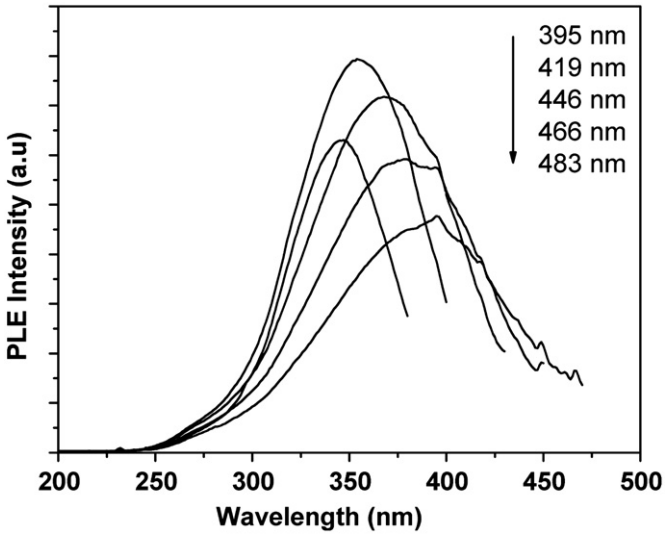

Fig. 13. PLE spectra of the ZnO/MPS nanocomposite recorded by monitoring emission wavelengths at 395, 419, 446, 466 and 483 nm.

nanoparticles [38]. Most recently, EWDP was also observed in polymellitic diimide nanowire network [39]. But very few reports were found in the literature on EWDP of ZnO nanoparticles. Recent reports show dependence of PL spectra of ZnO nanoparticles on excitation wavelength [36,40,41]. This kind of excitation wavelength dependent PL spectra was attributed to different phenomenon such as quantum confinement of the amorphous ZnO nanoparticles [39], amorphous structure and surface capping of ZnO nanoclusters [40], and salvation and energy transfer in the case of nano-ZnO colloids [42]. To identify the dependence of emission and excitation on particle size in the sample, PLE spectra were recorded by monitoring the emission wavelength (Fig. 13). As the monitored emission wavelength was increased, PLE spectra showed very interesting features such as decrease in intensity, broadening and redshift. PLE spectrum showed highest intensity when the emission wavelength was monitored at 419 nm which corresponded to the excitation at 355 nm. So there is good correlation between emission and excitation spectra and they follow the mirror image rule. Redshift of the PLE spectrum indicates the particle size dependence of the emission and excitation spectra [39]. At shorter monitoring wavelengths (e.g. 395 and 419 nm) excitations only to band edge are possible. While the emission wavelengths were monitored at 446, 466 and 483 nm, carriers were excited to the trap states and result in a broad PLE spectrum. When there is large size distribution, there will be different interactions between ZnO nanoparticles surfaces and mesoporous silica, because different sizes of ZnO nanoparticles results in different surface activities. Consequently, there exists different interaction energies between ZnO nanoparticles and mesoporous silica and hence they would exhibit EWDP [42]. The EWDP in carbon quantum dots passivated with PEG_{1500N} was attributed to the size distribution and also to the distribution of different emissive sites on each passivated carbon dot [43]. Here in this study mesoporous SiO_2 plays the same role as PEG_{1500N} in the case of carbon dots. So this excitation wavelength dependent PL may be attributed to the effects from particles of different sizes in the sample and also distribution of different emissive sites on each passivated ZnO nanoparticle as predicted in the case of carbon quantum dots capped with PEG_{1500N}.

5. Conclusion

The influence of precursors, temperature, surface area and excitation wavelength on PL of ZnO/MPS nanocomposite was studied in detail. Very fine ZnO nanoparticles of nearly 2–3 nm have been prepared inside the pores of MPS. It is observed that high emission intensity can be achieved with zinc acetate. The blueshifted peak at 363 nm, confirmed the strong quantum confinement of ZnO nanoparticles. It was found that emission intensity is increased with increase in surface area of host medium. The EWDP observed in this nanocomposite is ascribed to the quantum confinement effects and distribution of different emissive sites on each ZnO nanoparticle.

Acknowledgments

The authors would like to express thanks to Prof. Sethupathi, Department of Physics, IIT Madras, India for providing the HR-TEM facility. The authors are also thankful to Prof. Bansal, Dean, Department of Physics, University of Hyderabad (UOH), AP, India for permission to use FE-SEM facility. Authors would also like to thank S. Ramasamy, Technical officer Gr-I and Elisa Fathima, CIF, Pondicherry University for their continuous support in PL measurements. Authors are gratefully acknowledged to Dr. N. Venkatathri,

Department of Chemistry, National Institute of Technology, Warangal, for his valuable suggestions.

References

[1] H.W. Kroto, J.R. Heath, S.C. O'Brien, R.F. Curl, R.E. Smalley, C60: Buckminsterfullerence, Nature 318 (1985) 162–163.

[2] D. Clery, Shining a Bright Light on Materials, Science 277 (1997) 1213.

[3] P.F. Barbara, Nanoscale materials (a special issue), Accounts of Chemical Research 32 (1999) 387.

[4] C.T. Kresge, M.E. Leonowicz, W.J. Roth, J.C. Vartuli, J.S. Beck, Ordered mesoporous molecular sieves synthesized by a liquid-crystal template mechanism, Nature 359 (1992) 710–712.

[5] M. Selvaraj, B.H. Kim, T.G. Lee, FTIR studies on selected mesoporous metallosilicate molecular sieves, Chemistry Letters 34 (2005) 1290–1291.

[6] D. Buso, P. Falcaro, S. Costacurta, M. Guglielmi, A. Martucci, PbS-doped mesostructured silica films with high optical non linearity, Chemistry of Materials 17 (2005) 4965–4970.

[7] M. Wark, H. Wellmann, J. Rathousky, Homogeneously distributed CdS and CdSe nanoparticles in thin films of mesoporous silica, Thin Solid Films 458 (2004) 20–25.

[8] C. Bouvy, F. Piret, W. Marine, B.L. Su, Preparation, photoluminescent properties and quantum size effect of ZnS nanoparticles @ mesoporous silica CMI-1, Chemical Physics Letters 433 (2007) 350–354.

[9] B.J. Aronson, C. Blanford, A. Stein, Solution-phase grafting of titanium dioxide onto the pore surface of mesoporous silicates—synthesis and structural characterization, Chemistry of Materials 9 (1997) 2842–2851.

[10] W.H. Zhang, J.L. Shi, L.Z. Wang, D.S. Yan, Preparation and characterization of ZnO clusters inside mesoporous silica, Chemistry of Materials 12 (2000) 1408–1413.

[11] H.G. Chen, J.L. Shi, H.R. Chen, J.N. Yan, Y.S. Li, Z.L. Hua, Y. Yang, D.S. Yan, The preparation and photoluminescence properties of ZnO-MCM-41, Optical Materials 25 (2004) 79–84.

[12] Q. Lu, Z. Wang, P. Wang, J. Li, Structure and luminescence properties of Eu^{3+} doped cubic mesoporous silica thin films, Nanoscale Research Letters 5 (2010) 761–768.

[13] K. Wantala, S. Sthiannopkao, B. Srinameb, N. Grisdanurak, K.W. Kim, Synthesis and characterization of Fe-MCM-41 from rice husk silica by hydrothermal technique for arsenate adsorption, Environmental Geochemistry and Health 32 (2010) 261–266.

[14] L.I. Burova, D.I. Petukhov, A.A. Eliseev, A.V. Lukashin, Y.D. Tretyakov, Preparation and properties of ZnO nanoparticles in the mesoporous silica matrix, Superlattices and Microstructures 39 (2006) 257–266.

[15] P.B. Lihitkar, S. Violet, M. Shirolkar, J. Singh, O.N. Srivastava, R.H. Naik, S.K. Kulkarni, Confinement of zinc oxide nanoparticles in ordered mesoporous silica MCM-41, Materials Chemistry and Physics 133 (2012) 850–856.

[16] W. Zeng, Z. Wang, X.F. Qian, J. Yin, Z.K. Zhu, ZnO clusters in situ generated inside mesoporous silica, Materials Research Bulletin 41 (2006) 1155–1159.

[17] S.J. Pearton, D.P. Norton, K. Ip, Y.W. Heo, T. Steiner, Recent progress in processing and properties of ZnO, Progress in Materials Science 50 (2005) 293–340.

[18] B. Yao, H. Shi, H. Bi, L. Zhang, Optical properties of ZnO loaded in mesoporous silica, Journal of Physics: Condensed Matter 12 (2000) 6265–6270.

[19] Z. Fu, B. Yang, L. Li, W. Dong, C. Jia, W. Wu, An intense ultraviolet photoluminescence in sol–gel ZnO–SiO_2 nanocomposites, Journal of Physics: Condensed Matter 15 (2003) 2867–2873.

[20] G.Q. Tang, Y. Xiong, L.Z. Zhang, G.L. Zhang, Novel long-lifetime photoluminescence of nanosized ZnO included in the mesoporous MCM-41, Chemical Physics Letters 395 (2004) 97–102.

[21] F. Gao, S.P. Naik, Y. Sasaki, T. Okubo, Preparation and optical property of nanosized ZnO electrochemically deposited in mesoporous silica films, Thin Solid Films 495 (2006) 68–72.

[22] F. Gao, N. Chino, S.P. Naik, Y. Sasaki, T. Okubo, Photoelectric properties of nano-ZnO fabricated in mesoporous silica film, Materials Letters 61 (2007) 3179–3184.

[23] C. Bouvy, W. Marine, B.L. Su, ZnO/mesoporous silica nanocomposites prepared by the reverse micelle and the colloidal methods: photoluminescent properties and quantum size effect, Chemical Physics Letters 438 (2007) 67–71.

[24] C. Bouvy, E. Chelnokov, W. Marine, R. Sporken, B.L. Su, New phenomenon in the channels of mesoporous silicate CMI-1: quantum size effect and two-photon absorption of ZnO nanoparticles, Applied Physics A 88 (2007) 105–109.

[25] C. Bouvy, W. Marine, R. Sporken, B.L. Su, Photoluminescent properties of polyoxyethylene alkyl ether-type neutral surfactant templated mesoporous materials CMI-1: The absence of the 1.9 eV PL band, Chemical Physics Letters 420 (2006) 225–229.

[26] F. Piret, C. Bouvy, W. Marine, B.L. Su, A new series of optoelectronic nanocomposites: CMI-1 mesoporous core/ZnS shell, Chemical Physics Letters 441 (2007) 83–87.

[27] C.R. Shabnam, P. Arun Kanth, Controlling the photoluminescence of ZnO:Si nano-composite films by heat-treatment, Materials Research Bulletin 45 (2010) 1368–1374.

[28] R.M.S. Martins, V. Musat, A. Mucklich, N. Franco, E. Fortunato, Characterization of mesoporous ZnO:SiO_2 films obtained by the sol–gel method, Thin Solid Films 518 (2010) 7002–7006.

[29] K. Sowri Babu, A. Ramachandra Reddy, Ch. Sujatha, K. Venugopal Reddy, Effect of Mg doping on photoluminescence of ZnO/MCM-41 nanocomposite, Ceramics International 38 (2012) 5949–5956.

[30] H. Yang, Y. Deng, C. Du, Synthesis and optical properties of mesoporous MCM-41 containing doped TiO_2 nanoparticles, Colloids and Surfaces A: Physicochemical and Engineering Aspects 339 (2009) 111–117.

[31] M. Grun, K.K. Unger, A. Matsumoto, K. Tsutsumi, Novel pathways for the preparation of mesoporous MCM-41 materials: control of porosity and morphology, Microporous and Mesoporous Materials 27 (1999) 207–216.

[32] E. Caponetti, L. Pedone, M.L. Saladino, D. Chillura Martino, G. Nasillo, MCM-41-CdS nanoparticle composite material: Preparation and characterization, Microporous and Mesoporous Materials 128 (2010) 101–107.

[33] Q. Cheng, V. Pavlinek, Y. He, A. Lengalova, C. Li, P. Saha, Structural and elelctrorheological properties of mesoporous silica modified with triethanolamine, Colloids and Surfaces A: Physicochemical and Engineering Aspects 318 (2008) 169–174.

[34] W. Geng, R. Wang, X. Li, Y. Zou, T. Zhang, J. Tu, Y. He, N. Li, Humidity sensitive property of Li-doped mesoporous silica SBA-15, Sensors and Actuators B 127 (2007) 323–329.

[35] Y. Xiong, L.Z. Zhang, G.Q. Tang, G.L. Zhang, W.J. Chen, ZnO nanoparticles included within all-silica MCM-41: preparation and spectroscopic studies, Journal of Luminescence 110 (2004) 17–22.

[36] L. Irimpan, B. Krishnan, A. Deepthy, V.P.N. Nampoori, P. Radhakrishnan, Excitation wavelength dependent fluorescence behaviour of nano colloids of ZnO, Journal of Physics D: Applied Physics 40 (2007) 5670–5674.

[37] J.R. Lacowicz, Principles of Fluorescence Spectroscopy, third ed., Springer, New York, 2006.

[38] D. Pan, J. Zhang, Z. Li, C. Wu, X. Yan, M. Wu, Observation of pH-, solvent-, spin-, and excitation-dependent photoluminescence from carbon nanoparticles, Chemical Communications 46 (2010) 3681–3683.

[39] H. Zhang, X. Xu, H.F. Ji, Excitation-wavelength-dependent photoluminescence of a pyromellitic diimide nanowire network, Chemical Communications 46 (2010) 1917–1919.

[40] W.C. Zhang, X.L. Wu, H.T. Chen, J. Zhu, G.S. Huang, Excitation wavelength dependence of the visible photoluminescence from amorphous ZnO granular films, Journal of Applied Physics 103 (2008) 093718.

[41] B.S. Zou, V.V. Volkav, Z.L. Wang, Optical properties of amorphous ZnO, CdO, and PbO nanoclusters in solution, Chemistry of Materials 11 (1999) 3037–3043.

[42] A.B. Djurišic, Y.H. Leung, K.H. Tam, L. Ding, W.K. Ge, H.Y. Chen, S. Gwo, Green, yellow, and orange defect emission from ZnO nanostructures: influence of excitation wavelength, Applied Physics Letters 88 (2006) 103107.

[43] Y.P. Sun, B. Zhou, Y. Lin, W. Wang, K.A. Shiral Fernando, P. Pathak, M.J. Meziani, B.A. Harruff, X. Wang, H. Wang, P.G. Luo, H. Yang, M.E. Kose, B. Chen, L.M. Veca, S.Y. Xie, Quantum-sized carbon dots for bright and colorful photoluminescence, Journal of the American Chemical Society 128 (2006) 7756–7757.